Numerical Modeling of Bioluminescence Distributions in the Coastal Ocean*

IGOR SHULMAN

Naval Research Laboratory, Stennis Space Center, Mississippi

STEVEN H. D. HADDOCK

Monterey Bay Aquarium Research Institute, Moss Landing, California

DENNIS J. MCGILLICUDDY JR.

Woods Hole Oceanographic Institution, Woods Hole, Massachusetts

JEFFREY D. PADUAN

Naval Postgraduate School, Monterey, California

W. PAUL BISSETT

Florida Environmental Research Institute, Tampa, Florida

(Manuscript received 30 April 2002, in final form 31 January 2003)

ABSTRACT

Bioluminescence (BL) predictability experiments (predictions of the intensity, depth, and distance offshore of the BL maximum) were conducted using an advective–diffusive tracer model with velocities and diffusivities from a fine-resolution model of the Monterey Bay, California, area. For tracer initialization, observations were assimilated into the tracer model while velocities and diffusivities were taken from the hydrodynamic model and kept unchanged during the initialization process. This dynamic initialization procedure provides an equilibrium tracer distribution that is balanced with the velocity and diffusivity fields from the hydrodynamic model. This equilibrium BL distribution was used as the initial BL field for 3 days of prognostic calculations. Two cross-shore surveys of bioluminescence data conducted at two locations (north of the bay and inside the bay) were used in four numerical experiments designed to estimate the limits of bioluminescence predictions by tracers. The cross-shore sections extended to around 25 km offshore, they were around 30 m deep, and on average they were approximately 35 km apart from each other. Bioluminescence predictability experiments demonstrated a strong utility of the tracer model (combined with limited bioluminescence observations and with the output from a circulation model) in predicting (over a 72-h period and over 25–35-km distances) the location and intensity of the BL maximum. Analysis of the model velocity fields and observed and model-predicted bioluminesence fields shows that the BL maximum is located in the frontal area representing a strong reversal of flow direction.

1. Introduction

Prediction of the bioluminescence in the ocean represents a very challenging problem (Marra 1995): there is a lack of spatial and temporal coverage of available observations for robust model initialization; complex interactions characterize life cycles of autotrophs, grazers, and predators producing the bioluminescence (BL); little is known about the mathematical formulation and parameterization of the biological processes governing BL variability in a complex ecosystem, etc.

All of this limits the use of complex ecosystem models for BL predictions, with many degrees of freedom and uncertainty in the ecosystem model parameter specification. This high level of uncertainty may lead to difficulties in understanding and interpreting the model predictions. Some attempts at the prediction of bioluminescence have been made in one-dimensional settings. The model describing the relationship between BL, light intensity, and phytoplankton concentration was proposed by Ondercin et al. (1995).

In many instances, reliable, data-assimilating 3D circulation numerical models are available. They represent

* Naval Research Laboratory Contribution Number JA/7330/03/0009.

Corresponding author address: Dr. Igor Shulman, Naval Research Laboratory, Code 7331, Bldg. 1009, Stennis Space Center, MS 39529. E-mail: shulman@nrlssc.navy.mil

realistically the advective–diffusive as well as other physical processes in a particular area of the ocean. How much of the BL variability can be explained by the advective–diffusive processes of the tracer model combined with the circulation model and available limited BL observations? It is clear that the full temporal and spatial variability in BL structure cannot be explained by advection and diffusion alone within a tracer model. Source and sink terms, representing biochemical interactions and mortality rates, should be added, especially for relatively long-term predictions. For all mentioned above, the objective of this study is limited to evaluation of short-term forecasts (2–3 days) of bioluminescence, using limited BL observations with the tracer model (for modeling of BL) combined with the output from a circulation model. Moreover, our research is focused on the utility of the simple tracer model over short timescales in inferring and predicting the location and intensity of the BL maximum.

This paper has the following structure: in section 2 we outline the hydrodynamic model along with the forcing and formulations; observational BL data used in this study are described in section 3; in section 4, we present the results of the BL predictability numerical experiments; and in section 5 a discussion of results is presented.

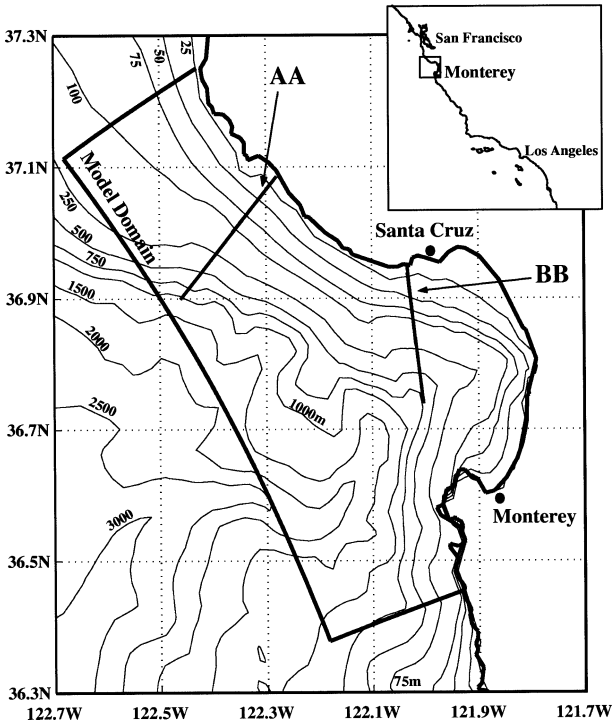

FIG. 1. Region around Monterey Bay, CA, showing the frsICON model domain, model-resolution bathymetry, and locations of sections AA and BB.

2. The hydrodynamic model

Bioluminescence predictability experiments were conducted by using tracer dynamics with velocities and diffusivities from the fine-resolution Innovative Coastal Ocean Observing Network (ICON) model (the frsICON model) of the Monterey Bay area. The model domain and bathymetry are presented in Fig. 1. The model grid (not shown) has a variable resolution in the horizontal, with finer resolution (500–600 m) around the upwelling front in the northern part of the Monterey Bay telescoping to coarser resolution (1.5 km) in the outer portion of the domain. The model has 30 vertical sigma levels. A three-dimensional, sigma-coordinate version of the Blumberg and Mellor (1987) hydrodynamic model is used. This free-surface model is based on the primitive equations for momentum, salt, and heat. It uses the turbulence closure submodel developed by Mellor and Yamada, and the Smagorinsky formulation is used for horizontal mixing. Additional information on the model can be found in Blumberg and Mellor (1987). The frsICON model is forced with atmospheric products from 9-km-resolution U.S. Navy Coupled Ocean and Atmospheric Mesoscale Prediction System (COAMPS; Hodur 1997) model predictions. Also, the frsICON model assimilates HF radar-derived surface currents (e.g., Paduan and Rosenfeld 1996). On the open boundaries, the frsICON model is one-way coupled to a larger-scale ICON Monterey Bay model (Shulman et al. 2000, 2002), developed by the ICON project (sponsored by the National Oceanographic Partnership Program). The ICON model is also based on the Blumberg and Mellor model (explicit, sigma-coordinate version) and has a variable horizontal resolution of 1–4 km. [See a detailed description of the ICON model in Shulman et al. (2002).]

In a one-way coupling scheme, the sea surface height and velocity from the coarser-resolution ICON model are used to specify open boundary conditions for the finer-resolution frsICON model. For temperature and salinity, the advectional boundary condition was used on the frsICON open boundaries [see, e.g., Shulman et al. (2002) for details on advectional open boundary condition]. According to the advectional open boundary condition, the temperature and salinity values from the coarser-resolution ICON model are advected into the frsICON model domain in the case of inflow, and the internal (one grid inside) frsICON temperature and salinity are advected to the frsICON open boundary in the case of outflow.

3. The bioluminescence data

Two nighttime surveys of bioluminescence data conducted along two transects (Fig. 1) were used in this study. The BL was measured using a custom-built bathyphotometer mounted on an Odyssey-type autonomous underwater vehicle (AUV). The details and specifications of the bathyphotometer will be the subject of another paper. Briefly the instrument pumps water into a

0.5-L sample chamber at a rate of 0.5 L s^{-1}. Flow rate, temperature, and light levels (photon flux, assuming isotropic emission) are measured in the sample chamber. The instrument is calibrated both radiometrically by a known light source, and biologically by insertion of a known amount of dinoflagellates. As with all bathyphotometers, only a fraction of the total luminescence is stimulated or sampled, but because organisms emit most of their light in the first part of their first flash, we capture a repeatable and representative fraction of the bioluminescence present in the environment. For the purposes of this study, this fraction (called simply ''bioluminescence'') is the property we are attempting to trace; in-depth descriptions of the biological and physical factors relating to bioluminescence will be presented in future manuscript. For the surveys, the vehicle undulated from the surface to the top 30 m of the water column as it covered the distance of at least 22 km.

The first cross-shore section was taken on the 242d calender day of 2000 in the northern part of Monteray Bay (labeled section AA in Fig. 1), and the second section was taken inside the bay on the 245th calendar day of 2000 (section BB). In Fig. 2 the observed BL distribution as a function of depth and distance offshore (in 10^9 photons per second) is shown for the AA and BB sections.

The observed BL maximum on day 245 (section BB) had a stronger intensity than the maximum for day 242 (section AA), and the location of the maximum on day 245 was shallower and closer to shore than that on day 242. In order to introduce some quantitative characteristics of the observed BL distributions, the BL fields were approximated with the following exponential function:

$$A \exp\left\{-\left[\frac{(z - z_o)^2}{(\Delta z)^2} + \frac{(d - d_o)^2}{(\Delta d)^2}\right]\right\}, \quad (1)$$

where A represents the intensity of the BL maximum, z_o is the depth of the maximum, d_o is the distance offshore of the maximum location, and Δz and Δd are length scales of the maximum spreading in depth and cross-shore distance, respectively. Table 1 shows the values of these parameters for sections AA and BB. The observed BL maximum for section BB is about 1.5 times stronger than the maximum for section AA. The section BB maximum is very shallow (7-m depth) and close to shore (6 km), while the section AA maximum is in deeper water (22-m depth) and 10–11 km offshore.

4. Bioluminescence predictability experiments

Bioluminescence predictability experiments were conducted using tracer dynamics with velocities and diffusivities from the frsICON model:

$$\frac{\partial C}{\partial t} = -u\frac{\partial C}{\partial x} - v\frac{\partial C}{\partial y} - w\frac{\partial C}{\partial z} + \frac{\partial}{\partial x}\left(A^h\frac{\partial C}{\partial x}\right) + \frac{\partial}{\partial y}\left(A^h\frac{\partial C}{\partial y}\right) + \frac{\partial}{\partial z}\left(K^h\frac{\partial C}{\partial z}\right) + S(x, y, z, t), \quad (2)$$

where u, v, w are components of velocity from the hydrodynamic model; A^h and K^h are horizontal and vertical diffusivities from the model; and $S(x, y, z, t)$ is the source minus sink term for C.

a. Initialization

In this section, the initialization procedure of (2) at day 242 is described. We start with the tracer concentration C equal to the background BL field (minimum of observed BL), and integrate Eq. (2) with the velocities and diffusivities taken from the hydrodynamic model at day 242 and kept unchanged during initialization. The BL observations are constantly assimilated by using the source term S in (2) in the following form:

$$S(x, y, z, t) = \gamma(C - C^o)\delta(\tau - \tau^o), \quad (3)$$

where C^o is BL observations (below we describe numerical experiments in which C^o represents different combinations of observed BL distributions from days 242 and 245; see Table 2), γ is the nudging coefficient, τ is the location in the model domain with coordinates (x, y, z), τ^o is the location of the observed BL (C^o) with coordinates (x^o, y^o, z^o), and $\delta(\tau - \tau^o)$ is a Dirac function for which $\delta = 1$ when $\tau = \tau^o$ and $\delta = 0$ otherwise.

In this case, the assimilated BL will be spread throughout the model domain according to the tracer dynamics (2) and the source term (3). Because the velocities and diffusivities do not change during the initialization procedure, the concentration C will reach equilibrium when the value of dC/dt is close to zero. This equilibrium will be achieved at every location in the model domain. In this case, the equilibrium state C_i will satisfy

$$-u_{242}\frac{\partial C_i}{\partial t} - v_{242}\frac{\partial C_i}{\partial y} - w_{242}\frac{\partial C_i}{\partial z} + \frac{\partial}{\partial x}\left(A^h_{242}\frac{\partial C_i}{\partial x}\right) + \frac{\partial}{\partial y}\left(A^h_{242}\frac{\partial C_i}{\partial y}\right) + \frac{\partial}{\partial z}\left(K^h_{242}\frac{\partial C_i}{\partial z}\right) + \gamma(C_i - C^o)\delta(\tau - \tau^o) = 0, \quad (4)$$

where subscript 242 means that variables are taken from the frsICON model predictions for day 242. Therefore, this dynamic procedure provides the equilibrium (C_i) tracer distribution that is balanced with the velocity and diffusivity fields from the hydrodynamic model on day 242.

At the locations of the observations, a balance is achieved between the advection and diffusion of tracers

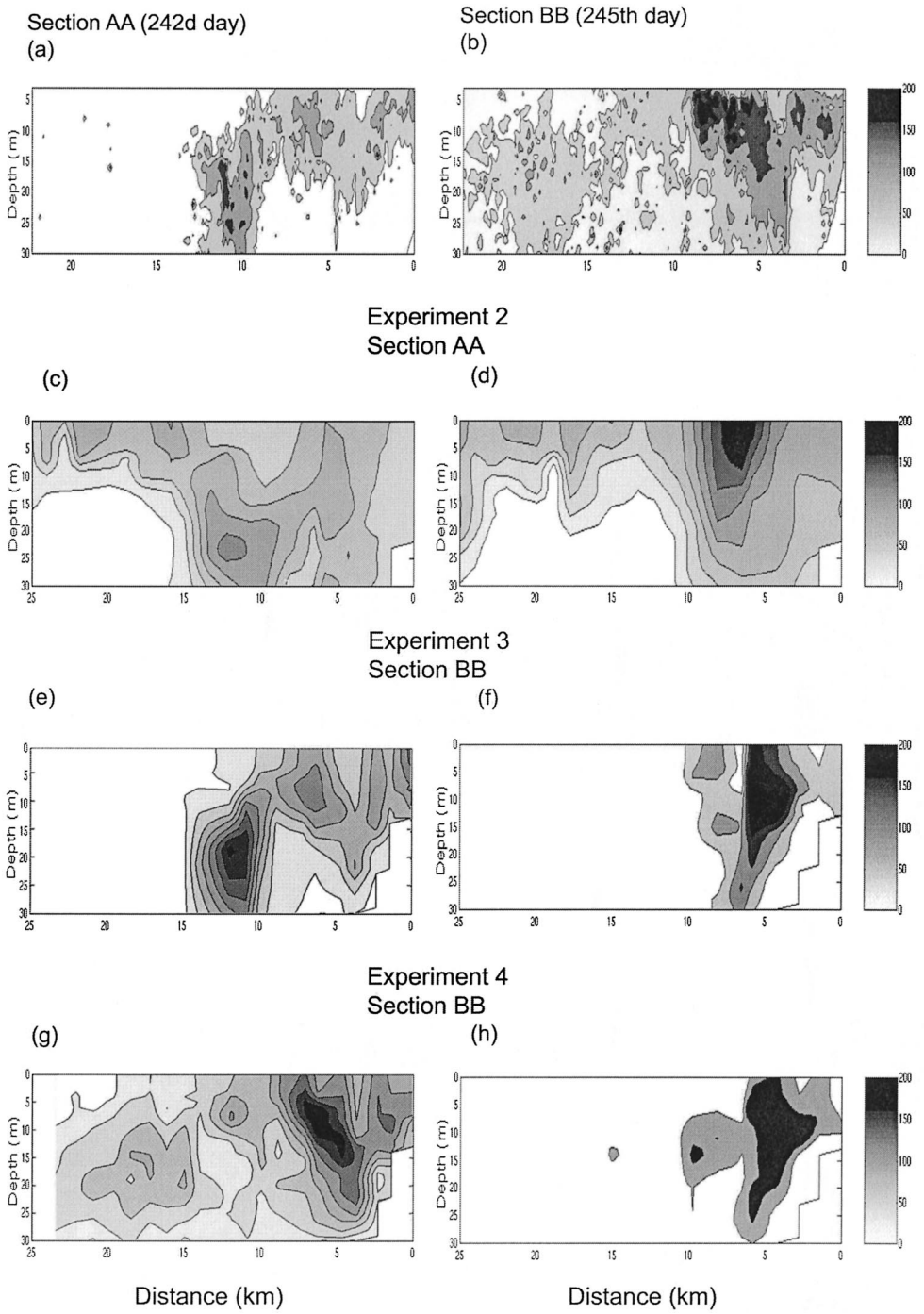

FIG. 2. Observed and model-predicted BL distributions (in 10^9 photons per second): (a) observed BL along section AA; (b) observed BL along section BB; (c) BL distribution at the end of initialization in expt 2; (d) BL distribution after 3 days of prognostic calculations in expt 2; (e) BL distribution at the end of initialization in expt 3 at section BB; (f) BL distribution after 3 days of prognostic calculations in expt 3; (g) BL distribution at the end of initialization in expt 4 at section BB; and (h) BL distribution after 3 days of prognostic calculations in expt 4.

TABLE 1. Numerical experiment results.

Cross sections	A	z_o	d_o	Δz	Δd
Observed, section AA	182.4	22.36	10.38	13.8	5.1
Observed, section BB	276.7	6.9	6.1	11.66	1.95
Expt 2, section AA, end of initialization	121.5	17.6	12.3	10.0	2.8
Expt 2, section AA, end of 72-h prognostic calculations	190.2	12.8	7.2	17.6	2.17
Expt 3, section BB, end of 72-h prognostic calculations	270.1	4.8	6.2	26.8	2.81
Expt 4, section BB, end of 72-h prognostic calculations	387.8	12.9	4.0	11.8	2.27

and the sink minus source term representing the misfit between the available bioluminescence observations and the model tracer distribution. In the rest of the model domain, the balance is achieved between the advection and diffusion of tracers. It is clear that observations along two transects are not sufficient for deriving initial 3D BL fields directly. It is nessesary to employ additional hypotheses in order to constrain the initialization problem. In the initialization procedure described, we employ the idea of dynamically balancing the tracer field with the velocity field. Dynamical balancing of velocity with temperature and salinity tracers is common procedure in the initialization of numerical physical models. This approach demonstrated good results in obtaining balanced initial physical fields, as well as in diagnostic calculations. However, we are not aware of any examples of such dynamical initialization for biological tracers. Although its biological implications are unclear, we view this as a practical means for initialization when lacking detailed observations of the 3D field of BL. Numerical experiments described below show that the location of the BL maximum can be recovered from this procedure at the time of initialization, and this balanced initial field provides good initial conditions for 3 days of prognostic calculations aimed at predictions of the location and intensity of the BL maximum.

There has been much discussion concerning the choice of nudging coefficient γ in (3). It was shown (Hines and Killworth 2001) that the long-term performance of data assimilation is relatively insensitive to the value of the nudging coefficient, and that smaller values of the nudging coefficient give a slower convergence to the steady state, which has similar properties when different values of nudging coefficient are chosen. In numerical experiments described below, the value of γ equal to 1/3600 s^{-1} was used, and our experiments with other values of γ also show a weak dependence of the equilibrium field C_i in (4) on the value of γ. In Hines and Killworth (2001), the following estimate of the timescale of tracer field convergence is presented: $(L/U)(A^h/UL)^{1/3}$, where L is length scale, U is velocity, and A_h is horizontal diffusivity. In our case, this scale is around 2.5 days. However, we integrated our model over at least 10 days in order to be sure that steady state was reached throughout the model domain.

TABLE 2. Numerical experiments.

	Initialization		Prediction
Expt	Data	Location	Location
1	242	AA	BB
2	245	BB	AA
3	242, 242	AA, BB	BB
4	242, 245	AA, BB	BB

The equilibrium tracer field (C_i) was used as the initial tracer distribution on day 242 for the following 3 days' prognostic calculations with tracer equation (2), where the source minus sink term is the last term on the left-hand side of Eq. (4) at the end of the initialization. During prognostic calculations, the hydrodynamic velocities and diffusivities change in accord with the hydrodynamic (frsICON) model.

On the open boundary of the frsICON model, we used the advectional open boundary condition for BL. The background BL values (minimum of observed BL) are advected into the frsICON model domain in the case of inflow, and the internal (one grid inside) frsICON BL values are advected to the open boundary in the case of outflow.

Below we describe the initialization and prognostic parts of four numerical experiments.

b. Numerical experiments

In order to gain insight into what predictability results to expect from numerical experiments, the oceanographic relationship between sections AA and BB was studied using finite-element particle-tracking software that permits tracking of Lagrangian particles in the circulation fields (Werner et al. 1993). Velocity fields from the ICON model, temporally averaged between days 242 and 245, were used in tracking particles both forward (Fig. 3, left) and backward in time (Fig. 3, right). Transect AA is located across a highly sheared region (Fig. 3) in which strong currents offshore are directed to the south–southeast. Just inshore, a coastal jet flows along the coast to the northwest. Particles placed along section AA tend to get entrained into the southeastward flow offshore due to an eddylike structure lying between the two current systems, and after 3 days of forward integration particles did not reach section BB inside Monterey Bay. This suggests that during days 242–245 water masses at section BB inside of the bay were not formed from water masses at section AA outside of the bay. Therefore, observations of BL collected on day 242 along AA outside of the bay will provide little infor-

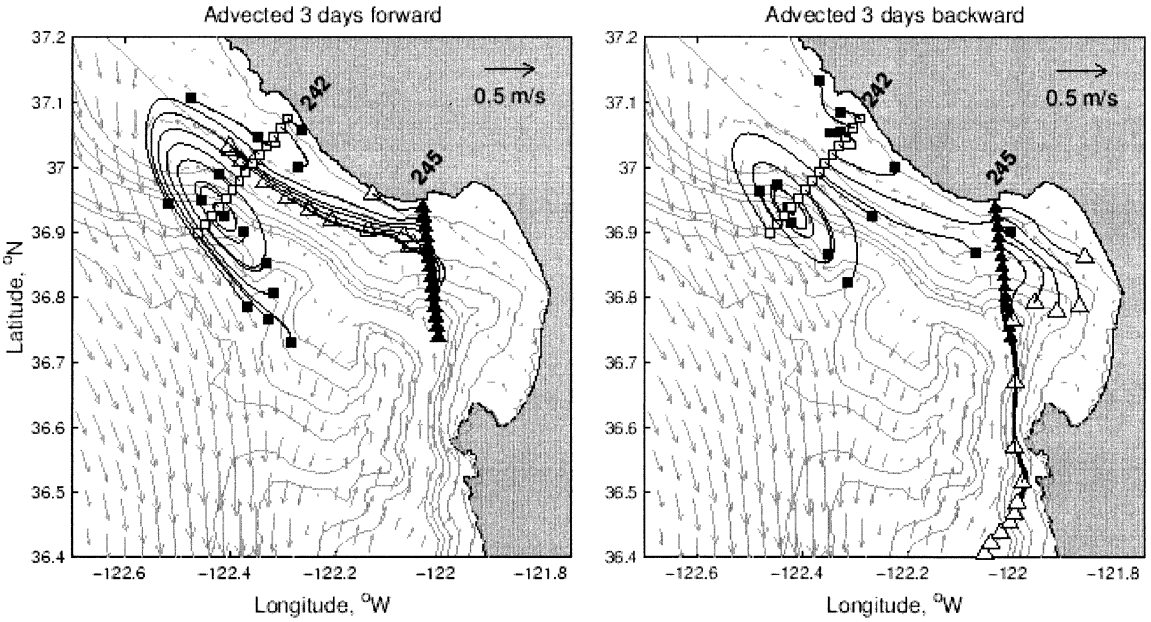

FIG. 3. Three days of (left) forward and (right) backward advection of particles placed along the AA and BB sections. Open and filled squares are the initial and final positions, respectively, of the section AA particles. Open and filled triangles are intial and final positions, respectively, of the BB section particles. Every fourth model velocity vector is plotted.

mation for short-term BL predictability inside the bay. According to Fig. 3, section BB feeds into a northward-flowing current at the mouth of Monterey Bay. Thus, backward advection of particles placed along section AA (Fig. 3, right) and forward advection of particles placed along section BB (Fig. 3, left) suggest that water masses along section BB inside the bay will reach section AA outside of the bay. This tells us that during days 242–245, sampling of BL intensity inside the bay plays an important role in BL predictability at section AA outside of the bay.

In the first two numerical experiments, the bioluminescence predictability at one of the cross-shore sections was investigated, by using the observed data at another section (see Table 2).

1) EXPERIMENT 1

The observed BL from section AA was assimilated to predict the BL maximum at the BB location. In this case, the function C^o in source term (3) had the following form:

$$C^o(x^o, y^o, z^o)|_{AA} = C_{AA}(d, z), \quad (5)$$

where $C_{AA}(d, z)$ is the BL distribution observed at section AA as a function of distance offshore (d) and depth (z).

The equilibrium initial field C_i in experiment 1 at the BB location, and the BL distributions after the following 3 days' prognostic calculations, were very different from the observed BL structure at this location. The advective and diffusive processes associated with the tracer model during days 242–245 were not able to spread the observed BL from the AA location to the area inside the bay. These results are consistent with the results from the particle-tracking experiments described above.

2) EXPERIMENT 2

In experiment 2, the observed BL from the BB location was assimilated to predict BL at the AA location. In this case, the function C^o in source term (3) had the following form:

$$C^o(x^o, y^o, z^o)|_{BB} = C_{BB}(d, z), \quad (6)$$

where $C_{BB}(d, z)$ is the BL distribution observed at section BB as a function of the distance offshore and depth.

Particle-tracking experiments (Fig. 3) suggest that BL assimilated along section BB in experiment 2 will reach the offshore section AA. The results of experiment 2 show that assimilation of only the BB survey data gives a good reconstruction of the BL structure observed at the AA location on day 242. In Fig. 2c the model BL distribution from experiment 2 at the end of initialization process [C_i in (4)] is shown at the AA location. There is a good agreement in the location of the BL maximum between the observed (Fig. 2a) and model predicted (Fig. 2c) BL distribution. In Table 1 (third row), the values of exponential function (1) for the C_i are shown. There is a good agreement in the locations of the BL maximum for the model-predicted and observed BL maximums (first and third rows).

The BL distribution at the AA location after 3 days

of prognostic calculations (on 245 day) is shown in Fig. 2d. After 3 days of prognostic calculations, the BL maximum moved closer to shore and became shallower. This is supported by the values for exponential function (1) presented in Table 1 (fourth row). If we compare the third and fourth rows of Table 1, we can see that after 3 days of prognostic calculations the location of the BL maximum in experiment 2 became shallower (from 17.6 to 12.8 m) and closer to shore (from 12.3 to 6.9 km offshore). Also, the intensity of the BL maximum was stronger after 3 days. This corresponds to the temporal and spatial tendencies in observed BL maximum distributions during days 242 and 245, although they were observed at different locations along the coast.

3) EXPERIMENT 3

In experiment 3, the observed BL structure along AA was assimilated at the AA and BB locations (Table 2). In this case, the hypothesis that BL as function of depth and offshore distance was the same at the AA and BB locations was introduced into the initialization problem. In this case the function C^o in source term (3) had the following form:

$$C^o(x^o, y^o, z^o)|_{\mathrm{AA}} = C_{\mathrm{AA}}(d, z)$$
$$C^o(x^o, y^o, z^o)|_{\mathrm{BB}} = C_{\mathrm{AA}}(d, z). \quad (7)$$

Initial distribution C_I and the model-predicted (after 72 h of prognostic calculations) BL fields at the BB location are shown in Figs. 2e and 2f. According to (7), the initialization field C_I resembles the observed BL structure at section AA. The predicted BL field reproduces the location and intensity of the observed BL maximum on day 245.

4) EXPERIMENT 4

In experiment 4, the observed BL structure at the BB location was assimilated on day 242 at this location (Table 2). In this case, the hypothesis concerning the time variability of the BL at the BB location was introduced into the initialization problem. In this case, the function C^o in source term (3) had the following form (Table 2):

$$C^o(x^o, y^o, z^o)|_{\mathrm{AA}} = C_{\mathrm{AA}}(d, z)$$
$$C^o(x^o, y^o, z^o)|_{\mathrm{BB}} = C_{\mathrm{BB}}(d, z). \quad (8)$$

Initial distribution C_I and the model-predicted (after 72 h of prognostic calculations) BL fields at the BB location are shown in Figs. 2g and 2h. According to (8), the initialization field C_I resembles the observed BL structure at section BB. As in experiment 3, the predicted BL field reproduces the location and intensity of the observed BL maximum on day 245.

In Table 1 (fifth and sixth rows), the values of the exponential function (1) for model-predicted BL fields in experiments 3 and 4 are shown. Experiments 3 and 4 were compared by using the following error metric:

$$\epsilon = \frac{\sum_{k=1}^{5} (P_k^o - P_k)^2}{\sum_{k=1}^{5} P_k^{o2}},$$

where P_k^o and P_k are, respectively, observed and model-predicted values of parameters in (1). The value of ϵ for experiment 3 is 0.06, while for experiment 4 it is 0.40. The results of the 3-day prognostic calculations show that the observed BL maximum location and intensity along the BB section are better predicted in experiment 3, in which the initialization procedure was based on the assumption that BL intensity as function of depth and offshore distance was the same at two cross-shore sections.

5. Discussion and conclusions

The presented numerical modeling experiments demonstrate the usefulness of the tracer model (combined with limited bioluminescence observations and with the output from a circulation model) in predicting the location and intensity of BL maxima. Because BL intensity was modeled using tracer dynamics, the hydrodynamic model velocities and diffusivities controlled the model BL distribution. In Fig. 4, plots of the model cross-section velocities are presented for days 242 and 245. During day 245, patterns of flow at AA as well as BB demonstrate the development of sharp fronts, which represent a reversal of flow direction, at around 7 km offshore. We would like to point out that during the prognostic calculations the strong BL maximum formed at around 7 km offshore, along section AA in experiment 2 (Fig. 2), and along section BB in experiments 3 and 4 (see Figs. 2e,f). Therefore, the locations of the observed and model-predicted BL maxima coincide with the location of the frontal area representing a reversal of flow direction. This suggests that the BL intensity is stronger in the area of the reversal of flow direction (around the eddylike structure). This statement can be supported by the following simple analytical consideration.

Let us consider an advective dominated flow [diffusion is insignificant and source term S is zero in (2)] and investigate properties of a stationary solution of (2). In this case, we have

$$-\mathbf{u} \cdot \nabla C = 0. \quad (9)$$

If $\tau_o = (x_o, y_o, z_o)$ is the location of the maximum of C at a particular time t, according to (9), velocity vectors will be orthogonal to the vectors of the gradient of C. Around the BL maximum, vectors of C gradients will have radial directions. Therefore, the velocity field around τ_o should have an eddylike structure. From this, and the good agreement between the observed and mod-

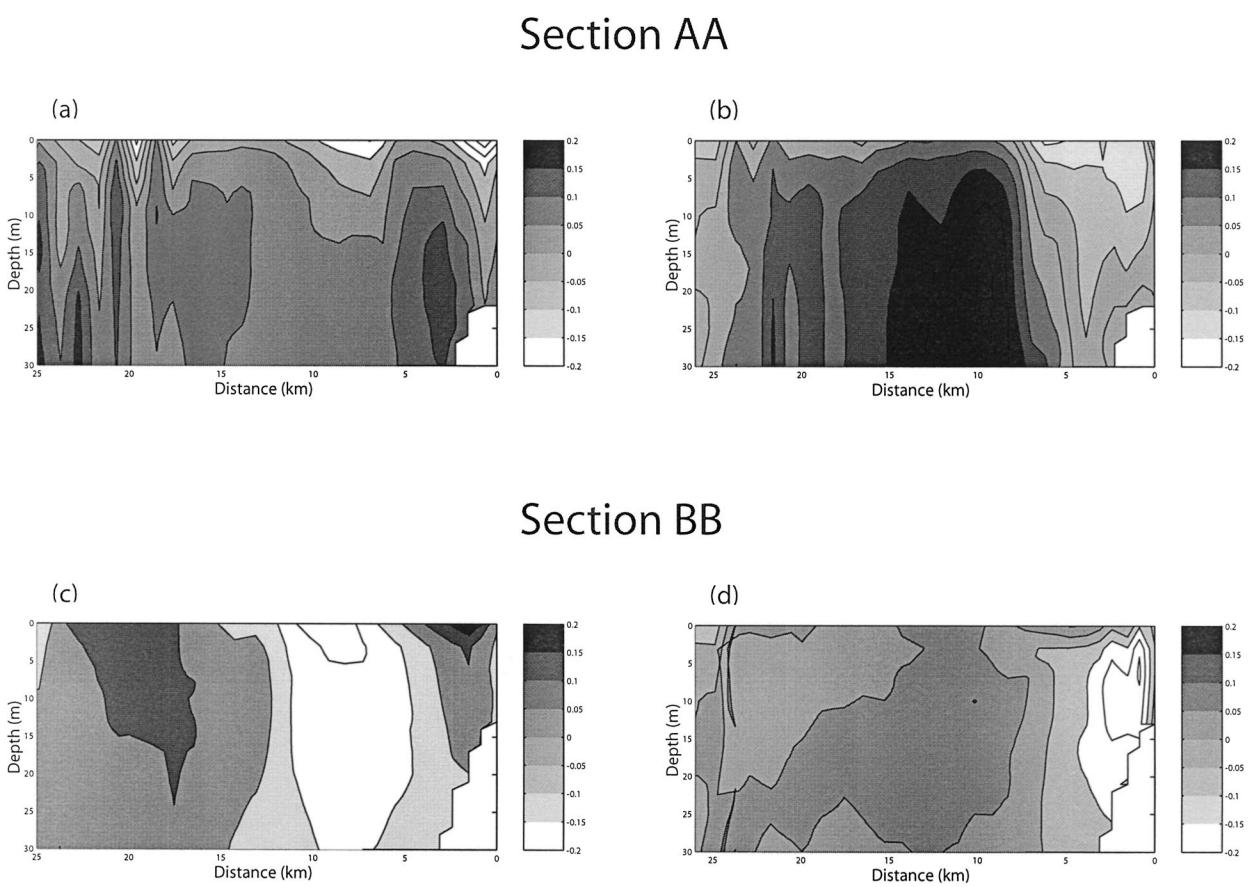

FIG. 4. Plots of the model alongshore velocities (m s^{-1}): (a) for day 242 at section AA; (b) for day 245 at section AA; (c) for day 242 at section BB; and (d) for day 245 at section BB.

el results, we can conclude that during days 242–245 advective processes can explain the offshore location of the BL maximum.

The results of our experiments suggest that short-term changes in some of the salient features in the coastal BL distribution can be explained by hydrodynamic transport processes. Without a doubt, biological dynamics will be important in longer-term predictions and could play a critical role in short timescale changes in some circumstances. Nevertheless, we suggest that numerical tracer experiments similar to those described herein should be conducted for the proposed locations and days of planned surveys. These numerical experiments will determine the influence of observed data on the predictability at other locations and allow the determination of optimal locations for the surveys. Our future research will be focused on the utility of such tracer experiments in helping to optimize limited BL sampling for maximum impact on BL predictions.

Acknowledgments. This work was supported by the Ocean Modeling and Prediction and Biological and Chemical Oceanography Programs of the Office of Naval Research. Shulman's component of funding is presently through the NRL 6.1 ''Use of a Circulation Model to Enhance Predictability of Bioluminescence in the Coastal Ocean'' project under Program Element 601153N sponsored by the Office of Naval Research.

Cyril Johnson and James F. Case of UCSB built and provided the bathyphotometer that was used to make measurements. Jim Bellingham and AUV technicians of MBARI maintained and operated the vehicles that were used to conduct surveys.

The authors would like to thank two anonymous reviewers for comments and suggestions. We also wish to thank Drs. Rosenfeld and Ramp of NPS for many helpful discussions. We thank Dr. Kindle of NRL and his group for providing open boundary data for the ICON model and atmospheric forcing for the ICON and frsICON models. Our thanks to Buckley Wilkinson of USM for significant help in figure preparation. Computer time was provided by grants of from the DoD HPC Center at the U.S. Naval Oceanographic Office, Stennis Space Center, Mississippi.

REFERENCES

Blumberg, A., and G. L. Mellor, 1987: A description of a three-dimensional coastal ocean circulation model. *Three-Dimensional*

Coastal Models, N. S. Heaps, Ed., Coastal and Estuarine Sciences, Vol. 4, Amer. Geophys. Union, 1–16.

Hines, A., and P. D. Killworth, 2001: An inversion–assimilation approach using hydrographic data in a coarse-resolution ocean model. *J. Atmos. Oceanic. Technol.,* **18,** 1503–1520.

Hodur, R. M., 1997: The Naval Research Laboratory's Coupled Ocean/Atmosphere Mesoscale prediction System (COAMPS). *Mon. Wea. Rev.,* **125,** 1414–1430.

Marra, J., 1995: Bioluminescence and optical variability in the ocean: An overview of the Marine Light-Mixed Layers Program. *J. Geophys. Res.,* **100,** 6521–6525.

Ondercin, D. G., C. A. Atkinson, and D. A. Kiefer, 1995: The distribution of bioluminescence and chlorophyll during the late summer in the North Atlantic: Maps and predictive model. *J. Geophys. Res.,* **100,** 6575–6590.

Paduan, J. D., and L. K. Rosenfeld, 1996: Remotely sensed surface currents in Monterey Bay from shore-based HF radar (Coastal Ocean Dynamics Application Radar). *J. Geophys. Res.,* **101,** 20 669–20 686.

Shulman, I., and Coauthors, 2000: Development of the high resolution, data assimilating numerical model of the Monterey Bay. *Estuarine and Coastal Modeling: Proceedings of the Sixth International Conference,* M. L. Spaulding and H. Lee Butler, Eds., 980–994.

——, C.-R. Wu, J. K. Lewis, J. D. Paduan, L. K. Rosenfeld, J. C. Kindle, S. R. Ramp, and C. A. Collins, 2002. High resolution modeling and data assimilation in the Monterey Bay area. *Cont. Shelf Res.,* **22,** 1129–1151.

Werner, F. E., F. H. Page, D. R. Lynch, J. W. Loder, R. G. Lough, R. I. Perry, D. A. Greenberg, and M. M. Sinclair, 1993. Influences of mean advection and simple behavior on the distribution of cod and haddock early life stages on Georges Bank. *Fish. Oceanogr.* **2,** 43–64.